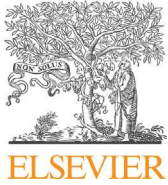


Energy dissipation during delamination in composite materials - An experimental assessment of the cohesive law and the stress-strain field ahead of a crack tip
Jalalvand M., Czél G., Fuller J. D., Wisnom M. R., Canal L. P., Gonzalez C. D., LLorca J.

This accepted author manuscript is copyrighted and published by Elsevier. It is posted here by agreement between Elsevier and MTA. The definitive version of the text was subsequently published in [Composites Science and Technology, 134, 2016, DOI: [10.1016/j.compscitech.2016.08.001](https://doi.org/10.1016/j.compscitech.2016.08.001)]. Available under license CC-BY-NC-ND.



Energy dissipation during delamination in composite materials – An experimental assessment of the cohesive law and the stress-strain field ahead of a crack tip



Meisam Jalalvand ^{a,*}, Gergely Czél ^{a,b}, Jonathan D. Fuller ^a, Michael R. Wisnom ^a, Luis P. Canal ^c, Carlos D. González ^{d,e}, Javier LLorca ^{d,e}

^a Advanced Composites Centre for Innovation and Science (ACCIS), University of Bristol, Queen's Building, University Walk, Bristol, BS8 1TR, United Kingdom

^b MTA–BME Research Group for Composite Science and Technology at Budapest University of Technology and Economics, Műgyetem rkp. 3., H-1111, Budapest, Hungary

^c LMAF, Ecole Polytechnique Fédérale de Lausanne (EPFL), Lausanne, Switzerland

^d IMDEA Materials Institute, C/ Eric Kandel 2, 28906, Getafe, Madrid, Spain

^e Department of Materials Science, Polytechnic University of Madrid, Madrid, Spain

ARTICLE INFO

Article history:

Received 22 March 2016

Received in revised form

22 July 2016

Accepted 1 August 2016

Available online 3 August 2016

Keywords:

Hybrid composites

Interface

Plastic deformation

Scanning electron microscopy

Traction-separation law

ABSTRACT

This paper presents detailed experimental information on mode-II delamination development in fibre/epoxy composite materials and provides observations about the process zone in the vicinity of the crack tip. It is shown that the energy dissipated in delamination propagation is spent on two ways (i) creating new fracture surfaces (delamination) and (ii) nonlinear shear deformation in the composite plies adjacent to the delaminating interface. Therefore, the nonlinear process zone is not restricted to the resin-rich interface between the layers, but also extends into the fibre/epoxy composite layers. This is different from the conventional assumption in modelling delamination using cohesive elements where the fibre/epoxy layers are fully linear-elastic and the process zone is lumped at the plane of fracture. Based on the accurately measured displacement field around the crack tip, the experimental traction-separation relation at the interface is found to be trapezoidal which is again different from the conventional bilinear cohesive law.

© 2016 The Authors. Published by Elsevier Ltd. This is an open access article under the CC BY license (<http://creativecommons.org/licenses/by/4.0/>).

1. Introduction

Delamination is a key limitation of composite materials. Occurrence of delamination is attributed to intrinsically low interfacial strength of laminated composites and usually results in loss of integrity of the structure and final failure. Several analytical approaches have been suggested to predict delamination. The initiation of delamination has been predicted by stress- or strain-based criteria [1,2], and other analytical approaches based on Fracture Mechanics have predicted delamination propagation due to free edges [3], static indentation [4] and fracture of the low strain material in Uni-Directional (UD) interlaminar hybrid composites [5]. However, it is necessary to find a way to numerically model delamination in more complicated problems.

It is widely accepted that cohesive (interface) elements along with interfacial cohesive laws can incorporate both stress-based criteria and Fracture Mechanics and is able to successfully model both initiation and propagation of delamination [6]. Implementation of the cohesive element approach is also quite straightforward and as a result, it has been successfully used for modelling different cases such as free-edge delamination [7,8], delamination induced by transverse cracks [9–11] and delamination in UD hybrid composites [12].

The mechanical response of cohesive elements is defined by the interfacial cohesive models known also as traction-separation laws. The area under the traction-separation law is assumed to be equal to the absorbed energy during fracture and is associated with the critical energy release rate. The interlaminar strength values are also used to set the maximum value of stress in the cohesive models.

Many of the quantitative experimental studies on cohesive models have investigated the de-bonding process of adhesively

* Corresponding author.

E-mail address: m.jalalvand@bristol.ac.uk (M. Jalalvand).

bonded joints to find the shape of the traction-separation law and also studied the effect of adhesive layer thickness [13–19]. An experimental method has been proposed in Refs. [16–18] to determine the relationship between stress and elongation of a thin adhesive layer between two steel sheets like a Double Cantilever Beam (DCB) loaded in pure mode I. A similar approach has been used for large scale fibre-bridging in DCB tests with UD laminates [20,21] by applying non-equal pure bending moments to each beam. To avoid the complexity of measuring crack length, a subtle modification was suggested in Ref. [22] and the J-integral values were calculated based on the applied moment and displacement at the end of the DCB.

All of the aforementioned experimental studies assume that all irreversible behaviour e.g. plastic deformation and damage, occur only at the adhesive or thin interface between the layers which do not experience any nonlinearity themselves. This is the same assumption as when cohesive elements are used for delamination modelling in the Finite Element (FE) approach and implies that the damage process zone is “planar” with zero thickness [23]. However, the assumption of a “planar” damage process zone has not been experimentally verified in composite materials, and there are experimental observations that do not agree with this assumption. Wisnom, Cui and Jones performed a number of tests on UD glass and carbon/epoxy specimens with cut central plies to study the effect of various factors on delamination [24,25]. They showed that the apparent interlaminar fracture toughness increases with the size of the specimen and depends on the geometry of the specimen. This conclusion is not intuitive if a planar damage process zone based on linear elastic fracture mechanics is assumed. Recently, Van Der Meer and Sluys [26] assumed a nonlinear shear response for the glass/epoxy layers and showed that significant parts of the adjacent layers around the delaminating interface experience nonlinear deformation and contribute to increasing the interlaminar toughness. This conclusion is also different from the conventional planar cohesive element assumption.

The aim of this paper is to study the phenomena of delamination initiation and propagation in monolithic composite materials at the layer interfaces and present new detailed experimental observations to further our understanding about the delamination development. For this purpose, UD carbon/glass hybrid specimens with cut central carbon layers are tested in tension and observed in-situ using a Scanning-Electron Microscope (SEM). High-resolution displacement fields are obtained through Digital Image Correlation (DIC) at different tensile load levels as described in Ref. [27]. The obtained high-resolution displacement fields are then used to

extract different parameters relating to the interfacial delamination such as the variation of separation between the layers, the shear strain and the shear stress at the interface and within the adjacent layers. The proposed method is fundamentally different compared to the available studies on traction-separation laws and is not based on any Fracture Mechanics assumptions.

It will be shown that significant parts of the layers adjacent to the delaminating interface experience high shear strains and contribute to energy absorption. This shows that the process zone ahead of the interlaminar crack has a “volumetric” rather than a “planar” shape and extends within the adjacent layers.

2. Experimental procedure

To achieve pure mode II delamination, UD glass/carbon hybrid composites with central cut carbon plies loaded in tension as schematically shown in Fig. 1 were selected. The specimen is designed for stable delamination at the glass/carbon interface at the applied tensile stress of 550 MPa [27] and then they were tested inside the vacuum chamber of a SEM to record a high resolution displacement field during delamination development and while the specimen is under load. This simple test avoids the large out of plane displacements of other standard mode-II fracture toughness tests such as End-Notched Flexure (ENF), making in-situ SEM imaging less complicated. Multiple images (tiles) covering the central part (~7 mm) of the specimen were recorded at subsequent nearly constant stress levels from zero up to the interlaminar crack propagation stress. The individual images were recorded with 10% overlaps suitable for later stitching of the tiles and to achieve a high resolution displacement field as shown in the bottom of Fig. 1 [27].

Fig. 1 shows a schematic of the specimen made up of 4 layers of Hexcel E-glass/913 epoxy on either side and 10 layers of thin SkyFlex USN 020A carbon layers in the middle. The thickness of each E-glass/epoxy ply is 0.144 mm and the SkyFlex carbon/epoxy ply is only 0.029 mm thick. The experimentally measured y-direction displacement obtained from DIC of 11 stitched SEM images taken at 428 MPa applied load is also shown in Fig. 1.

Both carbon and glass prepreg layers had a similar cure cycle with 120 °C maximum temperature. No further chemical details were provided by the suppliers but previous experimental studies [28,29] had confirmed compatibility, with a good adhesion between these different resin systems. The nominal free length of the specimens was 30 mm, and the nominal cross sectional dimensions were $1.5 \times 1.5 \text{ mm}^2$.

To study the delamination development, it is necessary to record

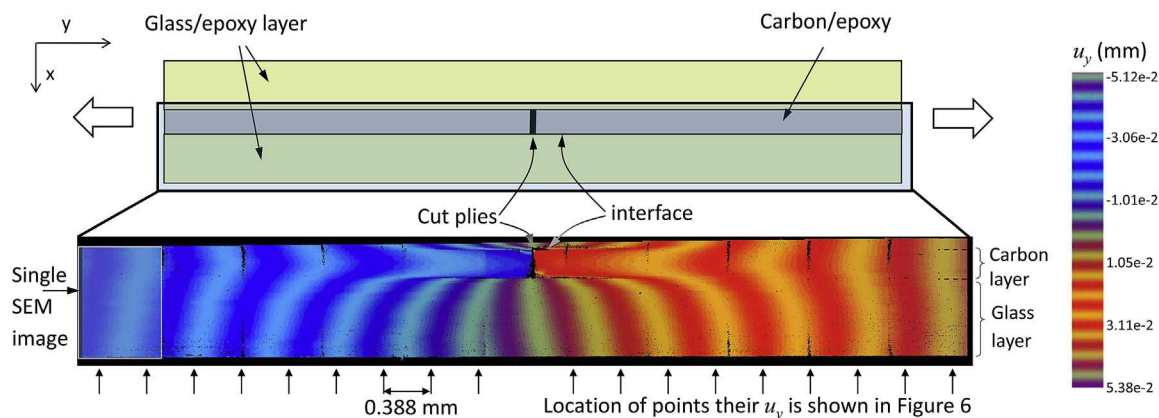


Fig. 1. Top view of a UD hybrid specimen with central cut carbon layers and the contours of the experimentally measured y-direction displacement (u_y) over the specimen at 428 MPa tensile load. Arrows indicate the location of points with equal distance from the cut for which u_y is shown in Fig. 6.

the displacement field while the specimen is under load. Therefore, the specimens were tested in-situ inside an SEM chamber and images were taken before delamination propagation at applied stresses of 428 MPa, 499 MPa, and 536 MPa. At each load, several digital SEM images were taken along the specimen and then stitched together to obtain an integral high resolution image of the delaminating interfaces and adjacent layers. Only one of the glass layers in addition to the full carbon thickness is covered in the SEM images to maximise the spatial resolution of the images. The acquired digital images were correlated (DIC) to find the full displacement fields at the load-steps with 3.91 μm spatial resolution. The details of the novel procedure for specimen preparation, testing, in-situ SEM imaging and the measurement of the full displacement fields of the delaminating interfaces are presented in Ref. [27]. In the present study, the displacement field is taken as an input and the interlaminar separation, shear strain distribution and interlaminar shear stress values are found.

The selected configuration has some similarities to a double-lap joint in terms of its symmetry at the mid-plane. However delamination propagation is more stable in UD laminate specimens with central cut plies than double lap ones allowing for step-by-step analysis of delamination.

3. Characterising delamination parameters—Post-processing methods

The main parameters that help to understand the delamination phenomena are the separation across the interface, the shear strain and stress at the interface as well as within the layers close to the interface. In this section, the post-processing method to obtain these parameters is discussed and in the following section, the obtained experimental results are presented.

3.1. Separation

Before delamination initiation, the interface is intact and both layers move together so the separation between the layers is zero. When the shear stress around the interface increases enough, the interface starts to deteriorate and a higher gradient of y-direction displacement is observed through the thickness around the cut. A delamination crack can be said to initiate when the displacement field has a discontinuity at the interface. Separation is the difference between the displacements of the adjacent layers and can be well estimated by subtracting the displacements of the centre of the facets at the edge of the adjacent layers, as shown schematically in Fig. 2. Usually 1 to 3 facets around the interface are not correlated by the DIC software (see Fig. 1, around the cut) because of field discontinuity or extensive distortion of the facets. But since the distance between the centres of neighbouring facets (grid spacing) is less than 4 μm, the deformation in these facets is negligible compared with the separation as will be discussed in the next section. Due to the small compressive stresses around the cut tips [25], the loading can be assumed to be pure mode II around the

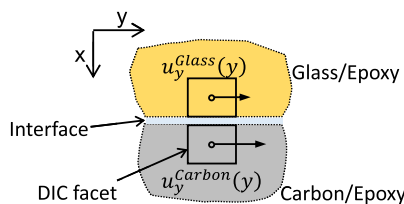


Fig. 2. Longitudinal displacement close to the interface causing pure mode-II separation.

crack tip. Therefore the separation between the layers is expected to have only a sliding component in the y direction (δ_y) as shown in Equation (1) and the opening mode-I component of the separation at the interface is expected to be zero, $\delta_x = 0$.

$$\delta_y(y) = u_y^{Carbon-edge}(y) - u_y^{Glass-edge}(y) \tag{1}$$

3.2. Shear strain within the composite layers

The loading is pure mode II so the shear strain, γ_{xy} , as defined in (2) is the most important strain component to study delamination.

$$\gamma(x,y) = \frac{\partial u_y}{\partial x} + \frac{\partial u_x}{\partial y} \tag{2}$$

The shear strain generally depends on displacement components in the x and y directions, but in this particular case, the through-thickness displacement component (u_x) was found to be negligible so the shear strain will only depend on displacement in the loading direction.

The initial assessments showed that the DIC results were slightly noisy, so 4th order polynomials were fitted to the u_y values of points at similar initial y-direction distances from the cut. Among different functions, this type of polynomial was found to give the best matching results. Fig. 3 indicates the good match of the original displacement and the curve fitted to the y-direction displacement of points 0.6 mm away from the cut on the carbon layer. Since the displacement field is discontinuous at the interface, the curve fitting process was carried out separately for points on the carbon layer and for the glass layers. The quality of the curve fitting for the full length of the specimen will be shown in Section 4, Fig. 6 and Fig. 7. The distribution of shear strain is found by differentiation of the fitted curve at different coordinates, $\gamma(x,y)$.

3.3. Shear stress at the interface

The stress at the interface is equal to the stress at the edge of the neighbouring layers which can be found using the shear strain values as input and then the shear constitutive law. If the material is linear-elastic, the distribution of shear stress can be found straightforwardly by multiplying the shear modulus by the shear strain distribution, $\tau_{xy} = G_{13}\gamma_{xy}$. However, fibre/epoxy composites show a nonlinear response in shear and as a result, the shear modulus, G_{13} , decreases as the shear strain increases. Using the transverse isotropy assumption for each ply, G_{13} and its variation can be estimated

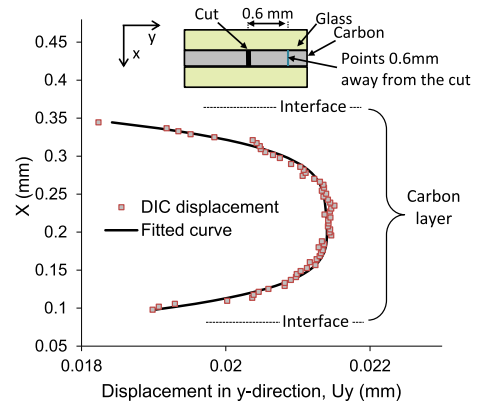


Fig. 3. Displacement of points 0.6 mm away from the cut and the curve fitted to filter out the noise.

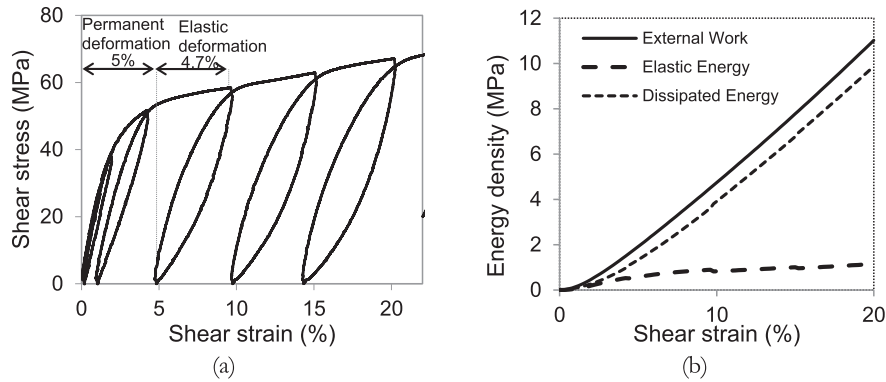


Fig. 4. (a) Loading-unloading shear stress-strain curve of $[\pm 45]_{5s}$ layup with thin SkyFlex USN 020A carbon layers (b) The density of external work, elastic energy and dissipated energy versus applied shear strain.

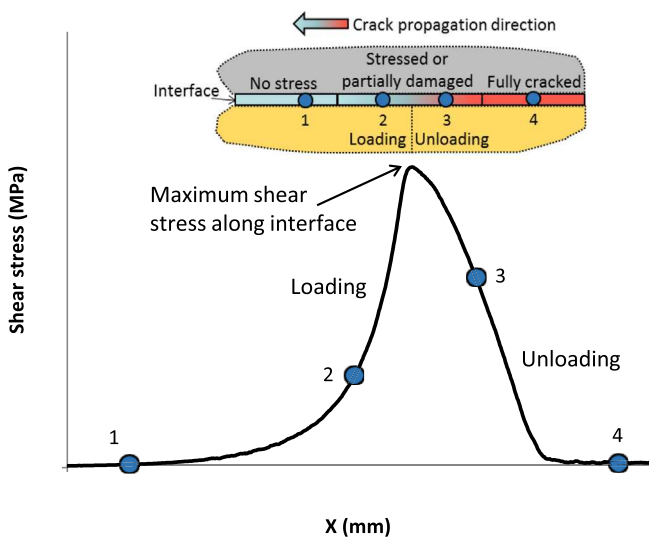


Fig. 5. Schematic shear stress variation at the interface from unstressed area to fully delaminated.

based on G_{12} values from a ± 45 shear test. A new set of tests with thin SkyFlex USN 020A carbon layers and $[\pm 45]_{5s}$ layup was performed. Fig. 4 (a) shows the experimental results of the loading-unloading shear test. Free-edge delamination was completely suppressed due to the low energy release rates associated with the thin-ply carbon/epoxy layers [30], so large shear strain values of more than 30% could be obtained. Due to the high shear strains achieved, it is necessary to take the fibre rotation into account as discussed in Ref. [30].

This set of results was used to work out the total external work applied on the material, the elastic energy density and dissipated energy density as shown in Fig. 4 (b). To find the dissipated energy for any maximum applied shear strain, a loading/unloading cycle was assumed and the area between the loading and unloading curves was taken as the dissipated energy density. The elastic energy density is equal to the area under the unloading curve. As shown in Fig. 4 (b), the amount of strain energy at shear strains above 2% is almost constant but the amount of dissipated energy increases almost with the same rate as the external work. This is mainly because at 2% strains and above, the shear stress-strain curve completely deviates from initial elastic straight line and the shear stress increases slightly with strain.

Along an interface with fully developed delamination, the

interface can be divided into three areas: i) fully delaminated interface, ii) stressed and partially damaged interface and iii) no interlaminar stress as shown in Fig. 5 where the variation of stress is also shown schematically. Similar shear stresses exist at the edge of the layers, next to the interface, which means that the material around the interface starts to take load as delamination propagates and after reaching the maximum value, the shear stress starts to drop and the material starts to unload. The shear strain at the edge of the layers also follows a similar pattern, starting at zero around the unstressed area, deformed to a maximum value in the process zone and then reducing in an unloading process zone. When there is nonlinear stress-strain behaviour, it is crucial to know if a point is in the loading or unloading phase in order to be able to find the stress from the strain, and also the value of maximum shear strain it has experienced, if it is in the unloading phase. This can easily be done by a global search for the maximum shear strain at the edge of the layers on each interface. The variation of shear strain at the edge of the layers is shown in Fig. 10 and will be discussed in detail later.

To check the validity of the approach, a series of 2D Finite Element simulations was run with the same geometry described in Section 2 using Abaqus. Cohesive elements were applied between the linear elastic glass/epoxy and carbon/epoxy layers. The displacements of all nodes just before stable delamination propagation were saved in a separate file. Then, a new file similar to the DIC displacement field format was produced from the FE displacement results file using a separate Matlab code. This new file was used as the input to the developed procedures for finding the separation, shear strain and stress as discussed in Sections 3.1–3.3. The obtained traction-separation law was very close to the one assumed in the FE modelling, confirming the validity and accuracy of this method. More details of this analysis can be found in Ref. [31].

4. Results

In this section, the parameters related to delamination, including the separation at the interface, shear strain and shear stress in the carbon/epoxy and glass/epoxy layers are presented using the methods discussed in Section 3.

The main displacement component over the whole specimen occurs along the loading direction, y axis. The separation, shear strain and shear stress values are all based on the distribution of this component around the cut. Fig. 6 indicates the raw displacement of individual points (u_y) on lines which were initially 0.388 mm apart in the y direction. The location of these lines is indicated with small arrows at the bottom of Fig. 1. Around the cut, the displacement of points in the carbon/epoxy layer is significantly larger than the displacement of the neighbouring glass/epoxy layer

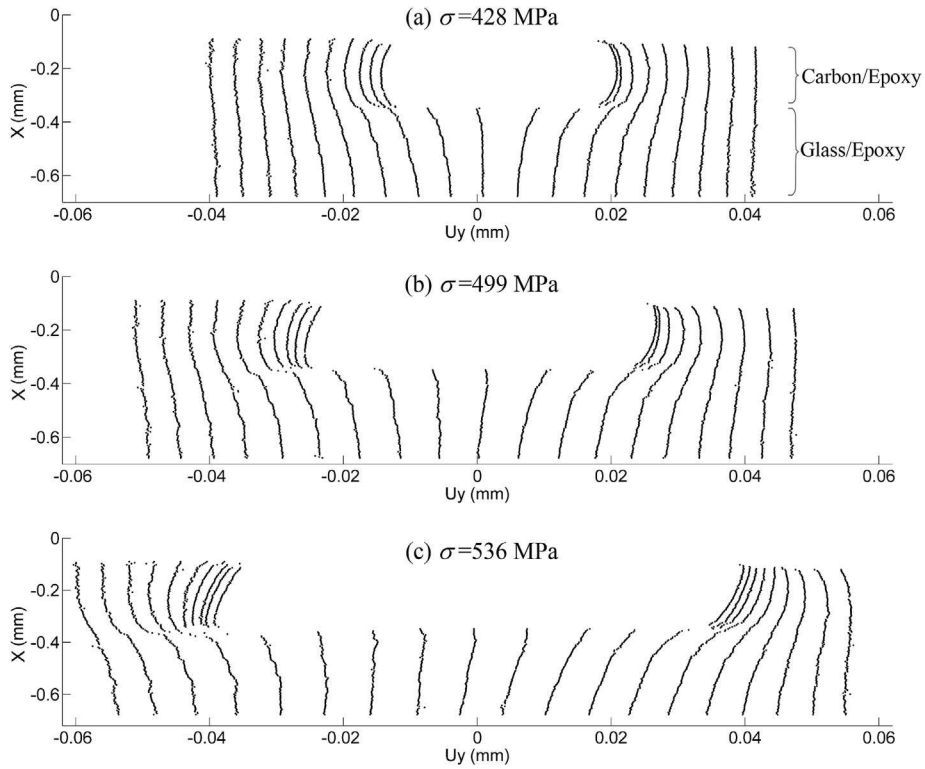


Fig. 6. Raw displacements of points 0.388 mm apart along loading direction (u_y) under (a) 428 MPa (b) 499 MPa (c) 536 MPa tensile far field stress.

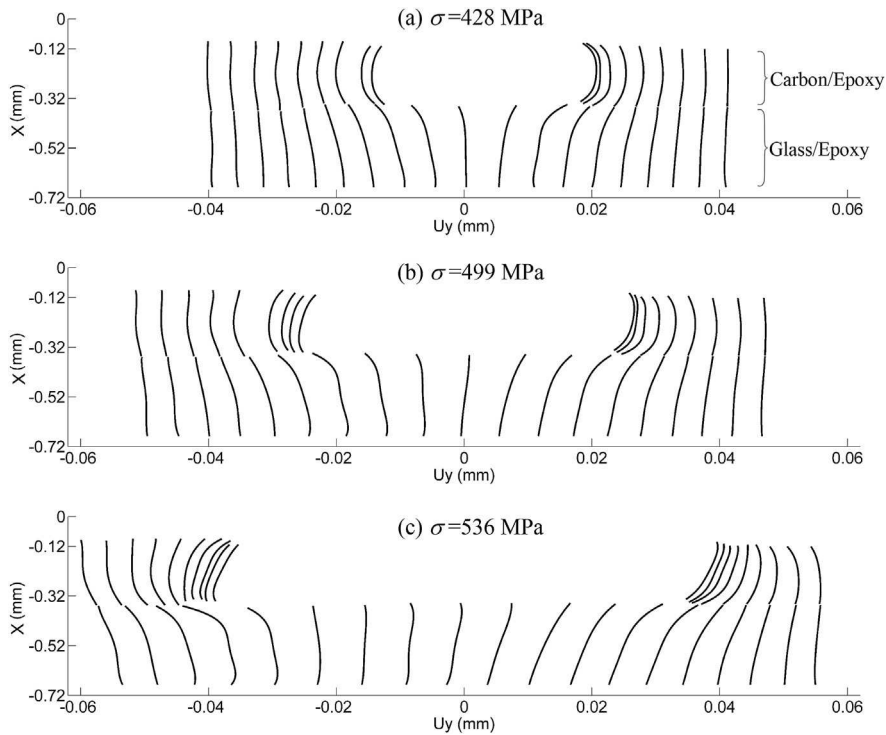


Fig. 7. Fitted curves used in smoothing procedure for loading direction displacements (u_y) at intervals of 0.388 mm apart under (a) 428 MPa (b) 499 MPa (c) 536 MPa far field tensile stress.

which can be interpreted as opening of the cut. The discontinuity between the points on glass/epoxy and carbon/epoxy layers at the interface close to the cut is clear and is an indication of interlaminar

separation and damage. But further away from the cut, the displacements of both glass and carbon layers are equal to each other showing that they are equally displaced in the y direction and there

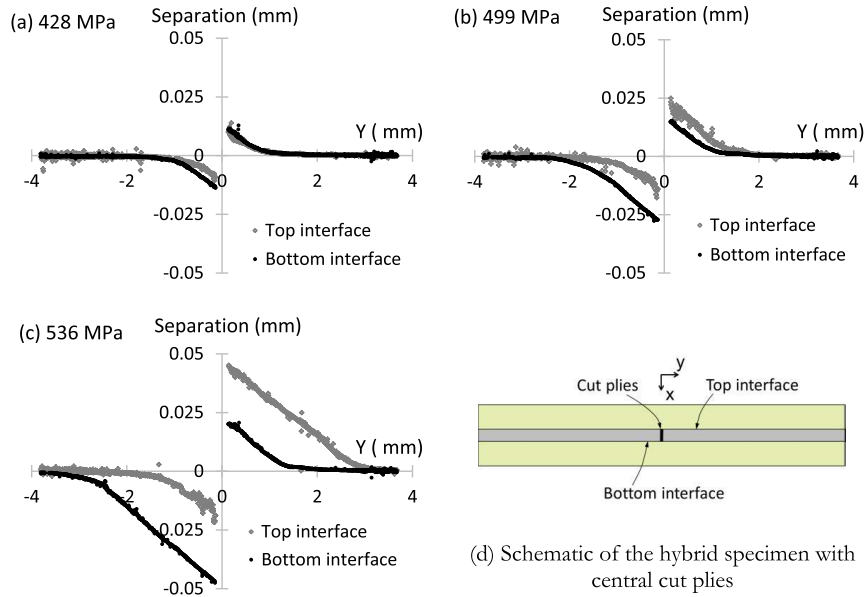


Fig. 8. Separation at the top and bottom interfaces versus distance from the cut at different applied stresses of (a) 428 MPa, (b) 499 MPa and (c) 536 MPa, (d) Schematic of the hybrid specimen with central cut plies.

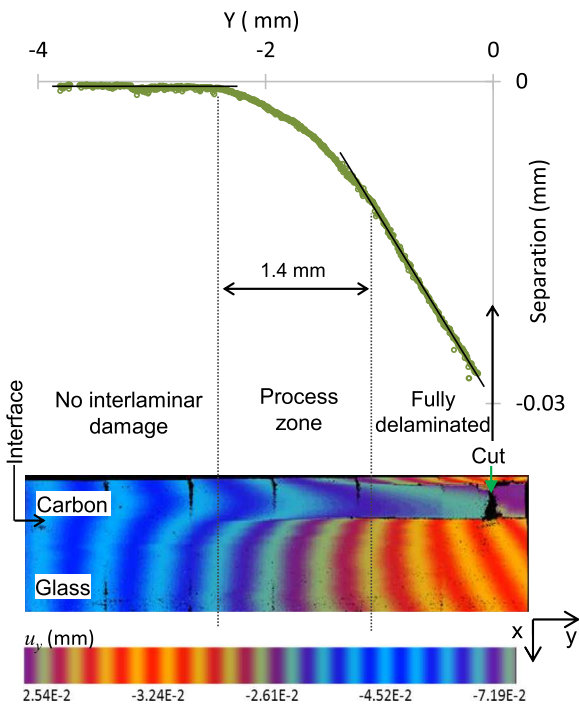


Fig. 9. Process zone, fully delaminated and intact areas highlighted on the separation variation of the bottom interface at 499 MPa applied stress.

is no separation between them.

The data shown in Fig. 6 is the original unsmoothed data. To calculate the shear strain and stress values, a curve fitting process to smooth the data as discussed in Section 3.2 and shown in Fig. 3 is implemented. Fig. 7 shows the curves fitted to the y-direction displacements of the points at intervals of 0.388 mm initial distance along the specimen. The similarity of Figs. 6 and 7 indicates the quality of the fitted curves over the whole specimen.

4.1. Separation of the interface

The value of separation between the glass/epoxy and carbon/epoxy layers is maximum at the cut and reduces further away. When there is no separation between the layers, the interface is intact whereas high values of separation means that damage has initiated at the interface. The variation of separation against distance from the cut for three different load levels is shown in Fig. 8 (a–c). No smoothing has been done and the obtained separation results are simply the subtraction of u_y from the correlated edge facets on the glass/epoxy and carbon/epoxy layers. The results are shown with single markers in grey and black for all facets along the top and bottom interfaces respectively as indicated in Fig. 8 (d).

At the lowest applied load of 428 MPa, the separation at both top and bottom interfaces are almost equal, showing the symmetry of the separation with respect to the mid-plane on both surfaces. But at higher load levels, the separations at the same distances on the top and bottom interfaces are different as shown in Fig. 8 (b) and (c). This non-symmetry is worse at 536 MPa where the separations at the top and bottom interfaces are about a factor of 2 different for points close to the cut.

The length of the process zone can be estimated from the variation of separation along the interface. The separation distribution of the bottom interface at 499 MPa stress is depicted in Fig. 9. Three different zones can be distinguished based on fitting straight lines to the beginning and end sections of the curve: i) fully delaminated interface, ii) stressed and partially damaged interface and iii) region with no interlaminar stress. In the bottom of Fig. 9, the distribution of deformation in the y-direction (u_y) for the same load and only the relevant part of the specimen is shown. The glass, carbon and interface layers are marked and the length of the specimen is matched with the y-axis on top.

Close to the cut, there is a clear distinction between the y-direction displacement (u_y) values in the carbon and glass layers, which indicates a significant displacement jump at the interface. Also there is no significant gradient of displacement in the carbon layer which means that this layer is not strained in the y-direction. The separation in this region is proportional to the distance from

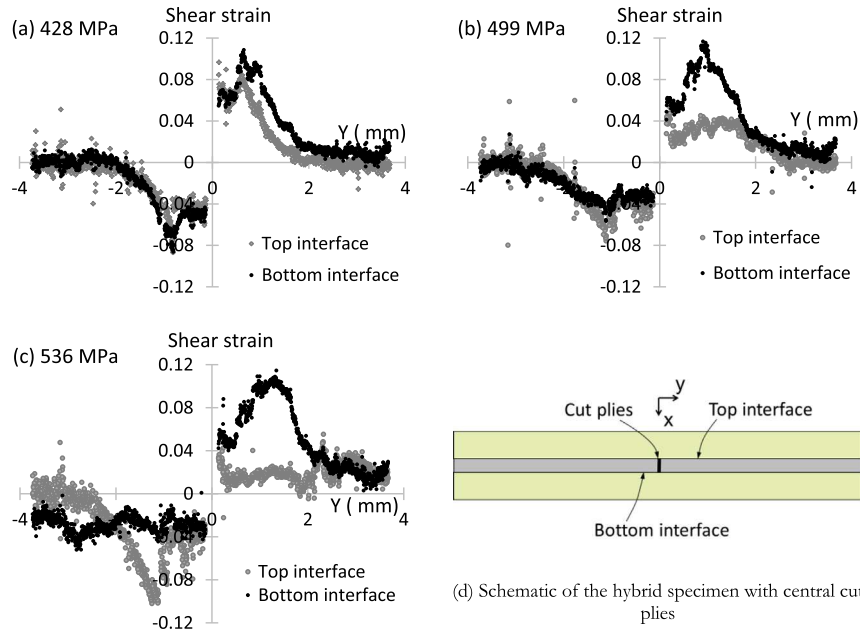


Fig. 10. Shear strain at the edge of the carbon layer along the top and bottom interface versus distance from the cut at different applied stresses of (a) 428 MPa, (b) 499 MPa and (c) 536 MPa, (d) Schematic of the hybrid specimen with central cut plies.

the cut and can be fitted with a straight line. Such a linear variation takes place when the glass layer uniformly elongates and the carbon layer stays at its initial length. This means that the interlaminar crack is fully developed and there is no shear stress between the glass and carbon layers. Faraway from the cut, there is no shear stress at the interface, the value of separation is theoretically zero and it can be correlated with a straight horizontal line. The process zone length is estimated to be around 1.4 mm. The very low non-zero separation value at points far away from the cut is only because of the non-symmetric delamination propagation, producing a small rotation of the specimen and can be neglected. The results in this figure are all original non-smoothed data obtained by subtracting u_y of the facets on either side of the interface as discussed in Section 3.1.

4.2. Shear strain at the edge of the carbon layer

As discussed earlier in Section 3.2, the slope of the fitted curves at the edge of the carbon layer represents the shear strain there. Fig. 10 (a–c) indicates the variation of this shear strain along the top

and bottom interfaces for the three applied loads. For 428 MPa tensile stress, the shear strain values along the interfaces are almost equal for points with similar distances from the cut. Far away from the cuts, the shear strain is equal to zero but it increases to a maximum value of about 9–10% at 0.7 mm from the cut. The shear strain then reduces at distances less than 0.7 mm to values of about 5%–6% at the cut.

At higher applied stresses, 499 MPa and 536 MPa, the shear strains at similar distances from the cut are not equal and their pattern along the x axis is not symmetric any more. This is similar to what has been observed in the separation distribution at higher loads and is due to asymmetric delamination along the top and bottom interfaces. Such asymmetry can also be seen in the y-direction displacement for the cases with higher tensile loads shown in Fig. 6 (b–c).

For 428 MPa applied tensile stress, where damage around the cut is symmetrical, it is possible to plot the shear strain variation at the edge of the carbon layer against interface separation as shown in Fig. 11 (a). The shear strain and separation are approximately proportional up to the maximum shear strain at 2–3 μm

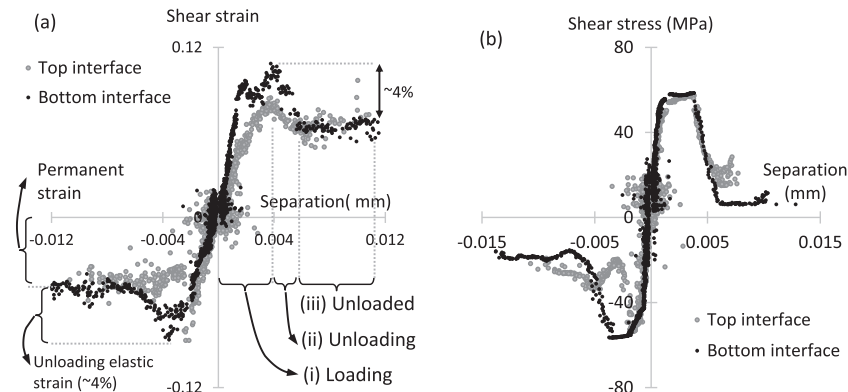


Fig. 11. (a) Shear strain at the edge of the carbon layer against interface separation at 428 MPa tensile stress (b) Shear stress versus separation obtained at 428 MPa tensile loading.

separation. At larger separations, the shear strain drops from the maximum value of about 9–10% to a constant value of about 5–6%. This clearly shows that the shear strain in the carbon layer along the interface has three phases: (i) a loading phase where the strain is increasing with separation, (ii) an unloading phase where the shear strain reduces with interface separation increase and, (iii) an unloaded phase where the shear strain is approximately constant. The drop in strain from the maximum value to the constant value at high separations in Fig. 11 (a) is about 4%. The shear test results shown in Fig. 4 (a) indicates that when the specimen was unloaded from 9.7% tensile strain, the elastic strain was about 4.7% and the specimen had almost 5% permanent deformation. These values are reasonably similar to the elastic and permanent deformation of the points at the edge of the carbon/epoxy layer and support the argument that these points have previously experienced higher shear strains and are now unloaded.

4.3. Shear stress at the interface

As shown in Fig. 4 (a), the carbon layer is highly nonlinear in shear and to find the shear stress at the interface, such nonlinear shear stress-strain relation should be used. As discussed in the previous section, the variation of shear strain versus separation has three phases: (i) a loading phase where shear strain and separation are proportional, (ii) an unloading phase where the shear strain reduces from the maximum value to an approximately constant value and (iii) a completely delaminated phase with no further change in shear strain as separation increases. The stress of the points in the loading phase can easily be found by using the shear stress-strain response of the material which is quite similar to the loading curves shown in Fig. 4 (a), but to find the value of shear stress in the unloading phase, it is important to know the maximum strain each point has experienced and is unloaded from. Finding the maximum shear strain each point individually has experienced is not possible. Therefore, it is assumed that the maximum shear strain of all points in the unloading phase is equal to the maximum shear strain along that half-interface. This maximum value on each half-interface was therefore used to separate the loading and unloading phases as shown in Fig. 11 (a) and then was used to work out the stresses in the unloading phase.

Fig. 11 (b) shows the obtained experimental traction-separation for 428 MPa tensile stress. The responses at both interfaces on the right and the bottom interface on the left are quite consistent but the top left interface is noisier. The shape of the traction-separation response is fairly similar to a trapezoid which is quite different from the conventional bilinear traction-separation laws usually used in FE modelling. For mode-II fracture of bonded joints, similar shapes of traction-separation behaviour have been reported [14,15].

In all four traction-separation curves (two for the top interface and two for the bottom interface), the final part has a small non-zero stress value. This might be for two reasons: friction and/or smoothing of the DIC data. Due to the compressive stresses around the cut tip, friction can apply some shear to the carbon layer. On the other hand, the smoothing process used for finding the shear strains slightly reduces the maximum shear strain value on each half-interface. With a slightly higher maximum value for the shear strain on each half-interface, the final parts of the traction-separation curves could be equal to zero.

4.4. Vicinity of the crack tips

Variation of the separation as well as the shear strain and stress of the carbon layer at the interface has been presented in Sections 4.1–4.3. In this part, the distributions of shear strain in the carbon/epoxy and glass/epoxy layers are presented. As discussed in Section

3.2, the slope of the curves fitted to the y-direction displacements (u_y) at different points with constant distance from the cut represent the shear strain. The same method is used here to work out the shear strain distribution within the whole layers and the results for the carbon/epoxy layer and a part of the bottom glass/epoxy layer at three different tensile stresses are shown in Fig. 12 (a). The shear strain in the top glass/epoxy layers was not plotted since that layer was not fully scanned by the SEM. The value of shear strain in the glass/epoxy layer far away from the interface is zero and therefore only a part of the glass/epoxy layer close to the interface is shown in Fig. 12 (a). Two separate curve fitting processes were applied for each carbon/epoxy and glass/epoxy layer. At the interface, there were usually a few missing facets in the DIC procedure, so the horizontal white lines between the carbon and glass/epoxy layers reflect the interface location. Around the cut, the DIC output data had several missing facets, so the curve fitting procedure was not accurate and the strains are not plotted. The narrower vertical white lines in the carbon/epoxy layers are again where the DIC process was not successful and the displacement of those points was not found. These lines are usually located at the boundary of SEM mosaic images stitched together with the procedure mentioned in Section 2. To show the shear strain variation through the thickness more clearly, different scales are chosen for the X and Y axes, as shown in the corner of Fig. 12 (a).

High gradient values of shear strain show the process zone where the material is deteriorating. At 428 MPa tensile stress, the highly sheared areas are quite close to the cut which means that the delamination process zone has not fully developed at this load. At higher loads, the highly sheared areas especially with positive shear strains have travelled away from the cut, which shows that delaminations at those areas have propagated. The distance between the areas with high positive shear strains and the cut is significantly larger than that between the areas of high negative shear strains and the cut (e.g. compare the positions of the red and blue areas at the bottom interface at 536 MPa tensile stress). This means that the delamination length on both sides of the cut is not symmetric. Such an asymmetry has also been observed directly in the SEM images.

Fig. 12 (a) indicates that a significant part of the thickness of each layer has been sheared more than 2%. According to the shear stress-strain response of the carbon layer shown in Fig. 4 (a), at shear strains larger than 2%, the shear response of the carbon/epoxy layer is largely inelastic. This means that a significant volume of the carbon/epoxy layer adjacent to the interface has experienced substantial nonlinear shear deformations. Such deformation absorbs energy in addition to the energy spent on producing the delamination fracture surfaces.

The variation of shear strain through the carbon layer thickness at 0.6 mm distance from the cut at 428 MPa stress is shown in Fig. 12 (b). The position of these points are highlighted with a red arrow in Fig. 12 (a) as well. The shear strain varies from 7.9% to –9.0% through the carbon layer thickness and about 0.050 mm of the total thickness on each side is sheared by more than 2%, experiencing nonlinear deformation according to Fig. 4 (a). The thickness of the carbon layer from the digital correlation images is 0.246 mm, which is 44 μm less than the nominal thickness. This is mainly because of missing facets close to the interface during the DIC procedure. Therefore, the thickness of the highly sheared area is even higher than the measured value of 50 μm on each side.

This observation is different from the conventional assumption applied in FE delamination modelling with interface/cohesive elements where each composite layer is assumed to behave in a linear elastic way and the cohesive elements are the only entity which has nonlinear behaviour. Fig. 12 (b) shows that about 30% of the volume of the carbon/epoxy layer has been sheared by more than 2% and therefore has experienced plastic deformation. Similar high shear

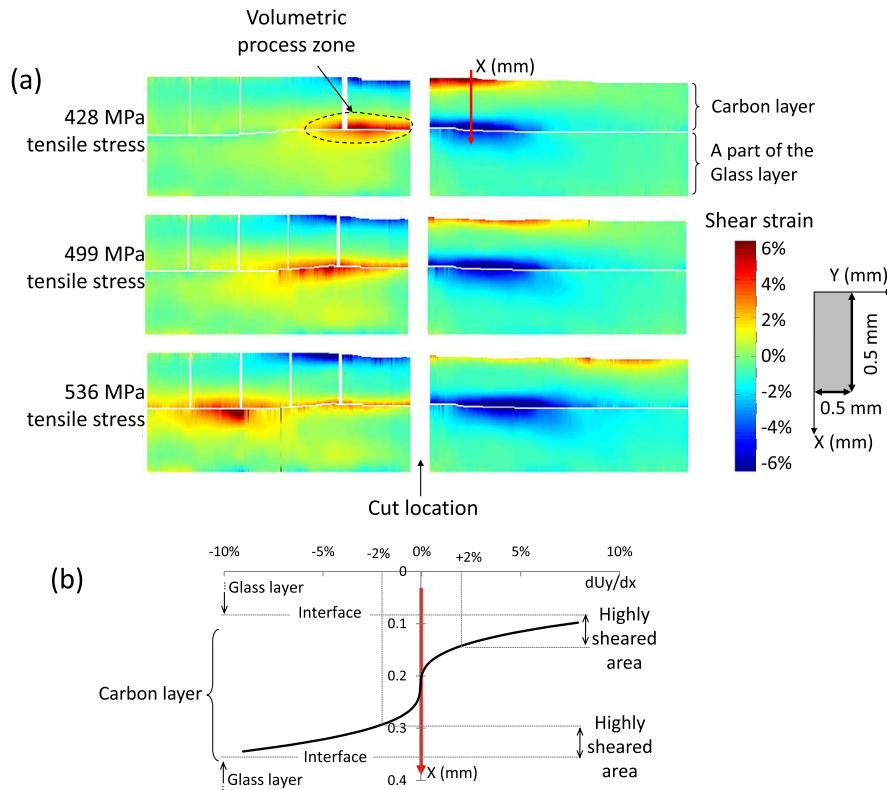


Fig. 12. (a) Shear strain distribution in the carbon and glass/epoxy layers (b) Shear strain in the carbon layer at a constant 0.6 mm distance from the cut at 428 MPa stress.

strain values are also seen in the glass/epoxy layers, close to the interface. The energy consumed by this nonlinear deformation is irreversible and contributes to the total dissipated energy during delamination propagation. Therefore, the process zone has a finite thickness of about one third of the whole carbon/epoxy layer thickness (100 μm) in total for both sides of the carbon layer rather than being confined close to the plane of fracture. This means that the process zone has a volumetric shape as shown in Fig. 12 (a).

The area under the traction–separation curves shown in Fig. 11 (b) is about 0.3 N/mm and is different from the typical G_{IIC} values for similar materials (about 1.0 N/mm) measured from energy release rate equations described in Ref. [25]. Such a big difference is for two main reasons: The load at which this curve was produced was less than the load at which delamination stably propagates and (ii) a part of the apparent toughness is due to the dissipated energy due to nonlinear deformation in the adjacent layers which is not included in the traction–separation response obtained from the interface. The reason for not evaluating the traction–separation law at higher loads is mainly because it was harder to identify a value for the maximum shear strain on the interfaces and therefore, the shear stresses were found to be less reliable. However, this does not affect the previous conclusion about the contribution of the carbon and glass layers to the apparent toughness of the material since that was independent of the shear stresses and was based only on the shear strain values that are believed to be accurate and reliable.

5. Discussion and conclusion

The test method used to determine the displacement field data [27] and the proposed post-processing method in this paper are novel approaches to obtain detailed information about delamination propagation. Compared to previous methods based on the J-

integral, the main advantage of this method is that it is not based on the assumptions of Fracture Mechanics and both the separation and shear strain values are found solely from the displacement field data. The shear stress values are also found using the experimental shear stress–strain curve so it involves less assumptions compared to previous approaches [16–18,20–22] and can help to understand the nature of the problem. This study has helped to provide a more profound knowledge about the displacements, strains and stresses in the vicinity of delaminations which is not necessarily consistent with the assumptions of conventional Linear Elastic Fracture Mechanics.

The full distribution of shear strain over the specimen surface (Fig. 12 (a–b)) shows that the process zone where material deteriorates and energy is dissipated extends well into the carbon/epoxy and glass/epoxy layers, and so has a finite volume. This observation contrasts with the conventional assumption in modelling delamination in composite laminates where the layers are assumed to be linear elastic, bonded by cohesive elements with zero or negligible thickness. In reality, the dissipated energy in the highly sheared areas of the composite layers adjacent to the delaminating resin rich interface adds to the energy dissipated in formation of new fracture surfaces. Both these parts of the dissipated energy are lumped together when the apparent fracture toughness is measured. The dissipated energy in the layer depends on the volume of the layers experiencing high shear strains and therefore depends on the absolute thickness of the material. This suggests that the measured apparent fracture toughness depends on the geometry of the specimen. The dependency of the apparent fracture toughness on the thickness of the layers in UD specimen with central cut was previously reported in Refs. [24,25] and was numerically studied in Ref. [26]. The findings in this paper are in agreement with those reports on such a dependency and provide

possible explanation of the effect.

The traction-separation law found in this study has a trapezoidal shape (Fig. 11 (b)) which is again different from the conventional bilinear ones usually applied in delamination modelling using cohesive elements.

Acknowledgment

This work was funded under the UK Engineering and Physical Sciences Research Council (EPSRC) Programme Grant EP/I02946X/1 on High Performance Ductile Composite Technology in collaboration with Imperial College, London, and by the EPSRC Building Global Engagements in Research grant EP/K004581/1 in collaboration with IMDEA Materials Institute. Gergely Czél acknowledges the Hungarian Academy of Sciences for funding through the Post-Doctoral Researcher Programme fellowship scheme, the János Bolyai scholarship and the Hungarian National Research, Development and Innovation Office - NKFIH for funding through grant ref. OTKA K 116070. The authors acknowledge Hexcel Corporation for supplying materials for this research. Due to confidentiality agreement with research collaborators and industrial partners, supporting data can only be available to bona fide researchers subject to a non-disclosure agreement. Details of how to request access are available at the University of Bristol's data repository: <http://doi.org/10.5523/bris.91unnvqibajq1kf7fhsat28yv>.

References

- [1] R.Y. Kim, S.R. Soni, Experimental and analytical studies on the onset of delamination in laminated composites, *J. Compos Mater* 18 (1984) 70–80.
- [2] J.C. Brewer, P.A. Lagace, Quadratic stress criterion for initiation of delamination, *J. Compos Mater* 22 (1988) 1141–1155.
- [3] T. O'Brien, Characterization of delamination onset and growth in a composite laminate, *Damage Compos Mater ASTM STP* (1982) 140–167.
- [4] G.A. Davies, P. Robinson, J. Robson, D. Eady, Shear driven delamination propagation in two dimensions, *Compos Part A Appl. Sci. Manuf.* 28 (1997) 757–765.
- [5] M. Jalalvand, G. Czél, M.R. Wisnom, Damage analysis of pseudo-ductile thin-ply UD hybrid composites - a new analytical method, *Compos Part A Appl. Sci. Manuf.* 69 (2015) 83–93.
- [6] M.R. Wisnom, Modelling discrete failures in composites with interface elements, *Compos Part A Appl. Sci. Manuf.* 41 (2010) 795–805.
- [7] H. Hosseini-Toudeshky, M. Jalalvand, B. Mohammadi, Delamination of laminates governed by free edge interlaminar stresses using interface element, *Key Eng. Mater* 385 (2008) 821–824.
- [8] J.C.J. Schellekens, R. De Borst, Free edge delamination in carbon-epoxy laminates: a novel numerical/experimental approach, *Compos Struct.* 28 (1994) 357–373.
- [9] M. Jalalvand, H. Hosseini-Toudeshky, B. Mohammadi, Numerical modeling of diffuse transverse cracks and induced delamination using cohesive elements, *Proc Inst Mech Eng Part C J Mech Eng Sci* 227 (2013) 1392–1405.
- [10] M. Jalalvand, H. Hosseini-Toudeshky, B. Mohammadi, Homogenization of diffuse delamination in composite laminates, *Compos Struct.* 100 (2013) 113–120.
- [11] M. Jalalvand, M.R. Wisnom, H. Hosseini-Toudeshky, B. Mohammadi, Experimental and numerical study of oblique transverse cracking in cross-ply laminates under tension, *Compos Part A Appl. Sci. Manuf.* 67 (2014) 140–148.
- [12] M. Jalalvand, G. Czél, M.R. Wisnom, Numerical modelling of the damage modes in UD thin carbon/glass hybrid laminates, *Compos Sci. Technol.* 94 (2014) 39–47.
- [13] G. Ji, Z. Ouyang, G. Li, Effects of bondline thickness on Mode-II interfacial laws of bonded laminated composite plate, *Int. J. Fract.* 168 (2010) 197–207.
- [14] Q.D. Yang, M.D. Thouless, S.M. Ward, Elastic-plastic mode-II fracture of adhesive joints, *Int. J. Solids Struct.* 38 (2001) 3251–3262.
- [15] R.M.R.P. Fernandes, J.A.G. Chousal, M.F.S.F. de Moura, J. Xavier, Determination of cohesive laws of composite bonded joints under mode II loading, *Compos Part B Eng.* 52 (2013) 269–274.
- [16] B.F. Sørensen, Cohesive law and notch sensitivity of adhesive joints, *Acta Mater* 50 (2002) 1053–1061.
- [17] T. Andersson, U. Stigh, The stress-elongation relation for an adhesive layer loaded in peel using equilibrium of energetic forces, *Int. J. Solids Struct.* 41 (2004) 413–434.
- [18] M.F.S.F. de Moura, J.P.M. Gonçalves, A.G. Magalhães, A straightforward method to obtain the cohesive laws of bonded joints under mode I loading, *Int. J. Adhes. Adhes.* 39 (2012) 54–59.
- [19] C. Sarrado, A. Turon, J. Costa, J. Renart, An experimental analysis of the fracture behavior of composite bonded joints in terms of cohesive laws, *Compos Part A Appl. Sci. Manuf* 90 (2016) 234–242.
- [20] B.F. Sørensen, P. Kirkegaard, Determination of mixed mode cohesive laws, *Eng. Fract. Mech.* 73 (2006) 2642–2661.
- [21] L. Sorensen, J. Botsis, T. Gmür, L. Humbert, Bridging tractions in mode I delamination: measurements and simulations, *Compos Sci. Technol.* 68 (2008) 2350–2358.
- [22] M.F.S.F. de Moura, R.D.S.G. Campilho, J.P.M. Gonçalves, Crack equivalent concept applied to the fracture characterization of bonded joints under pure mode I loading, *Compos Sci. Technol.* 68 (2008) 2224–2230.
- [23] M. Elices, G.V. Guinea, J. Gómez, J. Planas, The cohesive zone model: advantages, limitations and challenges, *Eng. Fract. Mech.* 69 (2002) 137–163.
- [24] M.R. Wisnom, On the increase in fracture energy with thickness in delamination of unidirectional glass fibre-epoxy with cut central plies, *J. Reinf. Plast. Compos* 11 (1992) 897–909.
- [25] W. Cui, M.R. Wisnom, M. Jones, An experimental and analytical study of delamination of unidirectional specimens with cut central plies, *J. Reinf. Plast. Compos* 13 (1994) 722–739.
- [26] F.P. Van Der Meer, L.J. Sluys, A numerical investigation into the size effect in the transverse crack tension test for mode II delamination, *Compos Part A Appl. Sci. Manuf.* 54 (2013) 145–152.
- [27] G. Czél, M. Jalalvand, M.R. Wisnom, L.P. Canal, C.D. González, J. Llorca, Novel experimental procedure and determination of full displacement fields of delaminating composite layer interfaces for evaluation of the mode II cohesive law, *Eng. Fract. Mech.* 149 (2015) 326–337.
- [28] G. Czél, M.R. Wisnom, Demonstration of pseudo-ductility in high performance glass-epoxy composites by hybridisation with thin-ply carbon prepreg, *Compos Part A Appl. Sci. Manuf.* 52 (2013) 23–30.
- [29] G. Czél, M. Jalalvand, M.R. Wisnom, Demonstration of pseudo-ductility in unidirectional hybrid composites made of discontinuous carbon/epoxy and continuous glass/epoxy plies, *Compos Part A Appl. Sci. Manuf.* 72 (2015) 75–84.
- [30] J.D. Fuller, M.R. Wisnom, Pseudo-ductility and damage suppression in thin ply CFRP angle-ply laminates, *Compos Part A Appl. Sci. Manuf.* 69 (2015) 64–71.
- [31] M. Jalalvand, G. Czél, M.R. Wisnom, Extracting interlaminar cohesive laws from displacement field measurements, in: H. Kim, D. Whisler, Z.M. Chen, C. Bisagni, M. Kawai, R. Krueger (Eds.), *Proceedings of American Society for Composites 2014-twenty-ninth Technical Conference*. Composite Materials, DEStech Publications, Inc, 2014.